# Dense Wavelength Multiplexing of 1550 nm QKD with Strong Classical Channels in Reconfigurable Networking Environments

**N A Peters[1], P Toliver[1], T E Chapuran[1], R J Runser[2], S R McNown[2], C G Peterson[3], D Rosenberg[3], N Dallmann[3], R J Hughes[3], K P McCabe[3], J E Nordholt[3], and K T Tyagi[3]**

[1]Telcordia Technologies, One Telcordia Drive, Piscataway, NJ 08854, USA

[2] Laboratory for Telecommunications Sciences, College Park, MD 20740 USA

[3] Los Alamos National Laboratory, Los Alamos, NM 87545, USA

E-mail: nap@research.telcordia.com

**Abstract.** To move beyond dedicated links and networks, quantum communications signals must be integrated into networks carrying classical optical channels at power levels many orders of magnitude higher than the quantum signals themselves. We demonstrate transmission of a 1550-nm quantum channel with up to two simultaneous 200-GHz spaced classical telecom channels, using ROADM (reconfigurable optical add drop multiplexer) technology for multiplexing and routing quantum and classical signals. The quantum channel is used to perform quantum key distribution (QKD) in the presence of noise generated as a by-product of the co-propagation of classical channels. We demonstrate that the dominant noise mechanism can arise from either four-wave mixing or spontaneous Raman scattering, depending on the optical path characteristics as well as the classical channel parameters. We quantify these impairments and discuss mitigation strategies.

## 1. Introduction

Over the past decade, there have been significant advances in optical networking technology that have increased the configurability and transparency of fibre networks [1]. A key enabler of this evolution has been the successful development and wide deployment of the reconfigurable optical add drop multiplexer (ROADM) in core, metro and access networks. ROADMs move fundamental networking functions such as multiplexing and routing from the electronic domain to the optical domain. The resulting optical transparency permits the transport of high-speed communications signals using advanced optical modulation formats without requiring intermediate nodes to be upgraded [2]. It also opens up the prospect of supporting even more exotic optical signals, such as photonic qubits for quantum communications. The most mature quantum communications protocol, quantum key distribution (QKD) [3,4], offers the possibility of providing a highly-secure key establishment service across a network. Optical transparency removes a critical roadblock to sending quantum signals over previously opaque networks. However, transparency does not guarantee that quantum signals can coexist with high-power classical channels on a shared network and maintain sufficient fidelity between end users to support quantum services such as QKD.

While there have been several successful demonstrations of quantum technologies on optical fibre systems [5-21], many of these experiments have been performed over dedicated

network infrastructures. The focus of the work described in this paper is to understand under what conditions quantum signals (e.g., those used to perform QKD) may be able to coexist with signals typically found in enterprise or metro area telecom networks. Presently, such coexistence is a challenge as current networks may carry up to 80 classical dense wavelength division multiplexed (DWDM) channels on a 50-200 GHz frequency grid. While our previous work has demonstrated the compatibility of 1310-nm QKD with strong classical 1550-nm DWDM communications channels [13,21], there may be advantages in placing the QKD signals in the same low-loss 1550-nm transmission window with the classical signals. Potential advantages include increased signal reach for QKD and compatibility with infrastructure not transparent to or already occupied by 1310-nm signals. However, decreasing the wavelength spacing between quantum and classical signals substantially increases the background noise, placing more stringent demands on filtering.

A first demonstration of 1550 nm-based QKD with a single in-band classical DWDM signal was reported in [15], where the quantum and classical signals were spaced by either 400 or 800 GHz. The networking architecture assumed a static, point-to-point connection between a single QKD transmitter and a single QKD receiver. The authors of [15] conclude that the dominant impairment impacting QKD performance in their experiment was inadequate filter isolation of the single classical channel. While an important first step, we improve on their results in several important ways. First, we demonstrate sufficient filter isolation (>110 dB) to overcome the classical channel crosstalk found in [15]. Here, our improvements enable the use of 200 GHz channel spacing and, allow us to measure the transmission effects that can become fundamental limits to the coexistence of QKD with classical communications channels. Next, we explore the impact of up to two simultaneous classical channels co-propagating with the quantum channel. Finally, we remove the point-to-point constraint present in the previous QKD/DWDM experiments by using a ROADM network element, which has switching and multiplexing capabilities, to emulate a reconfigurable network. The addition of a ROADM network element opens up the possibility for transparent path reconfiguration between QKD endpoints, which can enable scalable quantum networking over metro-size regions [21] without requiring secured, optical-electrical-optical (OEO)-based key regeneration, which have been proposed by other groups [19].

Improved spectral filtering enables the identification and experimental mapping of the primary impairments to quantum signals from closely spaced co-propagating DWDM classical signals. We show that the dominant impairment can arise not only from Raman scattering as was previously shown [13] but also from four-wave mixing (FWM). These two sources of noise can be challenging to manage since they can fall directly in the center of a passband intended for ultra-low power optical channels for QKD, and one cannot use simple filtering approaches to entirely reject them. However, theoretical calculations enable us to design experiments where these two impairments may be studied in relative isolation from each other. Experimentally we explore channel spacing between the quantum and classical signals as close as 200 GHz, and theoretically we calculate the effects of spacing as close as 10 GHz. We measure the impact of the classical signals both with a single-photon detector and with a 1550 nm QKD system, both utilizing typical ns-gated InGaAs avalanche photo diodes (APDs). We demonstrate that the dominant noise mechanism depends on the optical path characteristics as well as the classical channel parameters, and discuss impairment mitigation strategies.

## 2. Physical impairments

Even though networks are becoming more transparent, which can allow for transmission of quantum channels through reconfigurable nodes, they are not necessarily free from impairments at quantum signal power levels. This is largely due to the fact that the classical communications infrastructure can operate properly in the presence of multi-channel linear crosstalk noise which

is 40 dB or more below the classical signal strength [22]. However, the difference between the launch power of a typical classical communications channel and a quantum signal can be >100 dB. Thus impairments tolerable in classical optical communications may have power levels many orders of magnitude higher than the power levels of quantum signals utilized for QKD. While in the present work, we are primarily concerned with FWM and Raman scattering, it is important to note that amplified spontaneous emission from optical amplifiers, insufficient isolation from classical signals, and other sources of light, can all play an important role in determining whether it is possible to support quantum communications such as QKD over a given fibre network. Regardless of the source, the presence of noise photons in the passband of a QKD receiver increases the error rate, which ultimately limits the range and key generation rates of QKD. The next two subsections describe how FWM and Raman scattering can give rise to noise that would significantly impact quantum signals co-propagating with classical wavelengths on the same optical fibre.

*2.1 Four Wave Mixing*

Four wave mixing arises from the interaction between two or more pump fields and the $\chi^{(3)}$ nonlinearity of the optical fibre. Three optical channels at frequencies $f_i, f_j$ and $f_k$ ($k \neq i, j$) mix through the fibre's third-order susceptibility, creating a new wave of frequency

$$f_{ijk} = f_i + f_j - f_k . \tag{1}$$

The peak power of the mixing product, $P_{ijk}$, is given by [23]:

$$P_{ijk}(z) = \frac{\eta D^2 \gamma^2 P_i P_j P_k \, \mathrm{e}^{-\alpha z}}{9\alpha^2} \left[1 - \mathrm{e}^{-\alpha z}\right]^2 , \tag{2}$$

where $P_i$, $P_j$, $P_k$ are the powers of each of the three input channels, $\alpha$ is the fibre attenuation, z is the propagation distance, $\gamma$ is the fibre nonlinearity, and $D$ is the FWM degeneracy factor. If all three channels present in the fibre are at unique frequencies, it is referred to as the nondegenerate case, and $D = 6$. If there are only two optical channels present, the four-wave mixing process is referred to as the degenerate case ($i = j$, $f_i = f_j$), and $D = 3$. The FWM efficiency is given by:

$$\eta = \frac{\alpha^2}{\alpha^2 + \Delta\beta^2} \left\{ 1 + \frac{4\,\mathrm{e}^{-\alpha z} \sin^2\left(\frac{\Delta\beta z}{2}\right)}{\left[1 - \mathrm{e}^{-\alpha z}\right]^2} \right\} , \tag{3}$$

where the phase matching factor $\Delta\beta$ is given by:

$$\Delta\beta = \beta_{ijk} + \beta_k - \beta_i - \beta_j . \tag{4}$$

The quantity $\beta$ is the propagation constant of the various input channels ($i$, $j$, and $k$) and the resulting mixing product ($ijk$). In typical DWDM systems, channels are assigned to an equally-spaced frequency grid, with spacings of 50, 100 or 200 GHz. As a result of the periodic spacing, the FWM product terms that are generated fall on the same grid - either on the DWDM channel frequencies themselves, or on other grid frequencies above or below those utilized by the DWDM system. In our analysis, we use two adjacent channels of equal power, thus $i = j$, $P_i = P_j = P_k$ and $D = 3$, resulting in two FWM product terms. One FWM product falls one channel below the lower frequency channel, and the other falls one channel above the higher frequency channel. Using the equations above, we can calculate the FWM power generated by two classical DWDM channels. Figure 1 plots the noise that falls within an adjacent passband for an average DWDM launch power level of 1 mW (0 dBm) per classical continuous wave (cw) channel. The adjacent channel of interest, fixed at 193.5 THz in the simulation provided here, is assumed for the QKD passband. We vary the channel spacing, $\Delta f$, between 10 GHz and 1000 GHz and compute the

FWM power falling within the QKD passband for both standard single-mode fibre (SSMF) and non-zero dispersion-shifted fibre (NZ-DSF) lengths of 1km and 25 km. Note that for simplicity, we ignore the impact of data modulation format. In addition, we only plot the peak FWM mixing power, and we neglect the oscillations in FWM efficiency that typically results from the product of the phase matching factor and the length in equation (3) above.

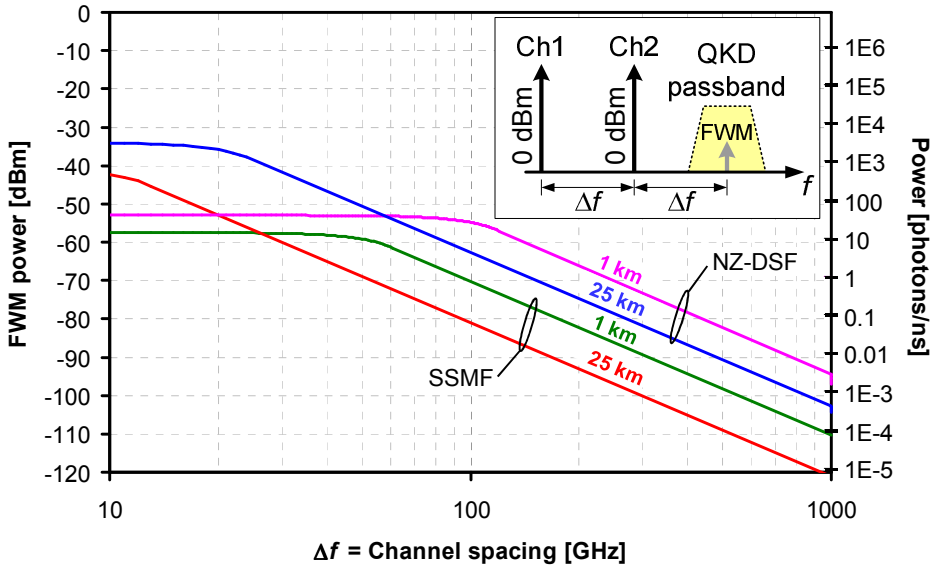


**Figure 1.** Calculation of adjacent channel FWM noise power generated by two 0-dBm cw lasers, plotted as a function of channel spacing for two different fibre types of 1 km and 25 km lengths. (SSMF=standard single mode fibre, NZ-DSF=non-zero dispersion shifted fibre)

As can be seen in the plot, the noise power is dependent upon channel spacing, fibre length, and fibre type. As a typical example, the calculated FWM noise for an SSMF fibre with a 200 GHz channel spacing between the 0 dBm DWDM channels is approximately -82 dBm at 1 km and approximately -92 dBm at 25 km.

To understand the potential impact of these noise levels on quantum communications signals, it is convenient to convert the power levels to an equivalent average photon number within a specified time interval. Noise levels expressed in the units of photons/nanosecond are helpful since single photon detectors in the telecom band are often operated using nanosecond gates. By this metric, the FWM noise from two 200 GHz-spaced 0 dBm signals corresponds to 5E-2 photons/ns and 5E-3 photons/ns at 1 km and 25 km, respectively. In contrast, using a 400 GHz channel spacing greatly reduces the FWM product powers yielding -94 dBm (~3E-3 photons/ns) and -103 dBm (~4E-4) for 1 km and 25 km, respectively. FWM product powers at the aforementioned levels can have a significant impact on QKD system performance because they can add substantial noise relative to the dark fibre case where the detector dark count rates on the order of 1 E-5/ns limit the system performance.

The preceding analysis has considered FWM products when only 2 classical channels are present. Clearly, this is a simplified case since 2 FWM products are generated, only one of which falls in the QKD passband. In general, with $N$ equally-spaced channels present, the number of mixing products is [22]

$$M = \frac{1}{2}\left(N^3 - N^2\right). \tag{5}$$

Assuming a set of $N$ contiguous equally-spaced DWDM channels ranging from $f_{\min}$ to $f_{\max}$, the mixing products are non-uniformly distributed over a wide spectrum of frequencies spanning both the original channels and side FWM product frequencies that extend all the way from:

$$f_{low} = 2f_{\min} - f_{\max} \quad \text{to} \quad f_{high} = 2f_{\max} - f_{\min} \tag{6}$$

As a result, the analysis of FWM impairments becomes considerably more complex. Future work will extend the results presented here to a more general case with larger numbers of classical channels.

*2.2 Raman Scattering*

Raman scattering arises from an inelastic interaction of a pump light with vibrational modes (optical phonons) in fibre. The scattered photons are generated at frequencies above and below that of the pump light, corresponding to anti-Stokes and Stokes scattering, respectively. The equations that govern the interaction between the pump, P, and another optical signal, S, due to the Raman process as a function of distance are as follows [24],

$$\frac{\mathrm{d}P}{\mathrm{d}z} = -\alpha_{\mathrm{P}}P + \beta_{\mathrm{P}}S + \gamma_{\mathrm{P}}PS \tag{7}$$

$$\frac{\mathrm{d}S}{\mathrm{d}z} = -\alpha_{\mathrm{S}}S + \beta_{\mathrm{S}}P + \gamma_{\mathrm{S}}PS \tag{8}$$

where $\alpha$, $\beta$, and $\gamma$ are the wavelength-dependent fibre attenuation, spontaneous Raman scattering coefficient, and stimulated Raman scattering coefficient, respectively. All three coefficients are given in per unit length. Since the pump and signal are at different wavelengths, the subscripts P and S are used to differentiate the fibre attenuation and scattering coefficients which are wavelength dependent. For the purposes of this study, the pump is generally one or more classical DWDM channels and the signal is the quantum channel. Since the quantum channel has very low power, the stimulated scattering terms (i.e., those with $PS$ products) and the signal's contribution to the pump ($\beta_{\mathrm{P}}S$) can be neglected. By requiring that the initial pump and signal launch powers at z=0 be $P(0)=P_o$ and $S(0)=0$, respectively, one can solve for the spontaneous Raman scattering power, S(z), at an arbitrary wavelength:

$$S(z) = \begin{cases} P_o\beta_{\mathrm{s}}z\mathrm{e}^{-\alpha_{\mathrm{P}}z} & \alpha_{\mathrm{P}} = \alpha_{\mathrm{S}} \\ P_o\dfrac{\beta_{\mathrm{S}}}{\alpha_{\mathrm{S}} - \alpha_{\mathrm{P}}}\left(\mathrm{e}^{-\alpha_{\mathrm{P}}z} - \mathrm{e}^{-\alpha_{\mathrm{S}}z}\right) & \alpha_{\mathrm{P}} \neq \alpha_{\mathrm{S}} \end{cases} \tag{9}$$

There are two important points to note from this equation. First, the spontaneous Raman noise is proportional to the initial launch power of the pump. Second, the fibre attenuation value at a particular wavelength is fixed. The consequence of these two effects is that the propagation distance is the only parameter which changes the amount of scattered light at a specific wavelength for a given launch power. The peak level of the Raman noise is reached at a propagation distance of

$$z_{\max} = \begin{cases} 1/\alpha_{\mathrm{P}} & \alpha_{\mathrm{P}} = \alpha_{\mathrm{S}} \\ \dfrac{1}{\alpha_{\mathrm{P}} - \alpha_{\mathrm{S}}}\ln\left(\dfrac{\alpha_{\mathrm{P}}}{\alpha_{\mathrm{S}}}\right) & \alpha_{\mathrm{P}} \neq \alpha_{\mathrm{S}} \end{cases} \tag{10}$$

At distances greater than $z_{max}$, the fibre attenuation diminishes the scattered noise signal more quickly than it can be replenished by the pump. By assuming narrowly spaced classical channels in the C-band with $\alpha_P \approx \alpha_S$ (0.185 dB/km), the Raman peak is to a very good approximation given by $1/\alpha_P$. Upon conversion to linear units by the factor ln(10)/-10, the predicted Raman noise peak is approximately 23.5 km. (In 3.3 and 4.2, we will experimentally explore the spontaneous Raman noise with photon counting measurements at a distance just beyond this maximum.)

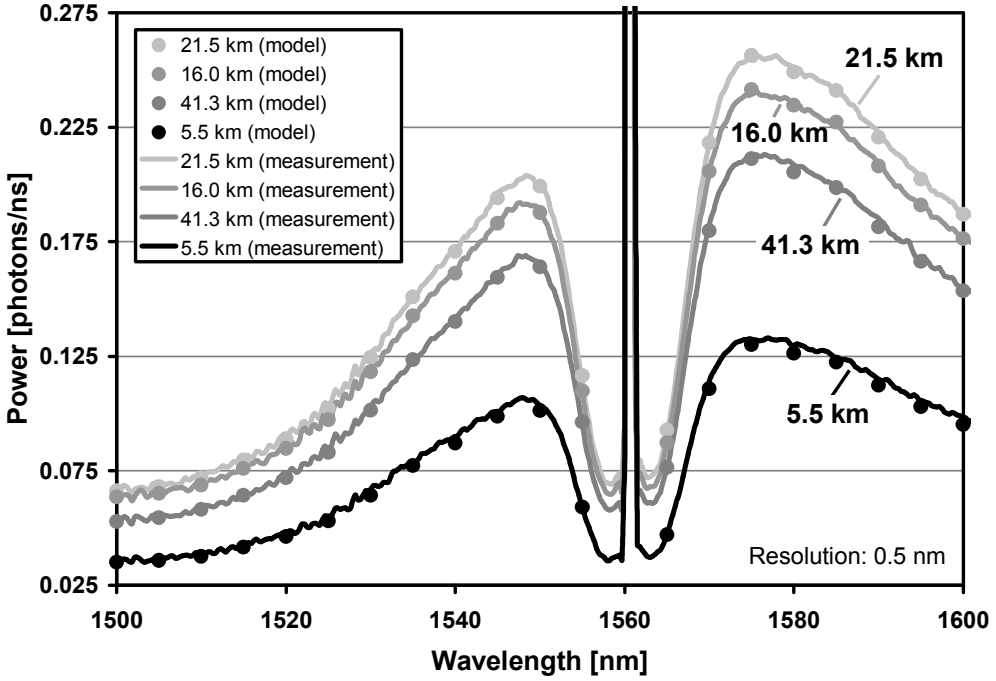


**Figure 2**. Measured and modeled Raman spectra generated by a cw pump passing though different lengths of standard single mode fibre. (Note the scale does not show the peak power at the center frequency of the cw pump.)

To understand the extent of the impact of Raman noise on quantum channels, we measure the Raman spectra generated by a 1560 nm cw pump propagating over several different fibre lengths of standard single-mode fiber (Corning SMF-28e®). The optical spectrum analyzer uses a bandwidth of 0.5 nm and the launched power of the cw pump is 0.84 dBm (1.2 mW). The 1560-nm pump is band-pass filtered using a narrowband (0.2 nm) grating filter to suppress the spontaneous emission noise from the laser to a level that is below the minimum sensitivity of the OSA (< -90 dBm) before being injected into the transmission fibre. Each segment of fiber is fusion spliced together to reduce the impact of connector losses on the measurement. The output from the fiber is passed through a double-stage fiber Bragg grating filter to notch out the pump by 40 dB. The notch filter enables the OSA to operate within its dynamic range limit at its minimum sensitivity. Figure 2 shows sample spectra of the spontaneous Raman noise for several lengths of fibre. The data was corrected to account for the residual spectral ripple and bulk insertion loss from the notch filter. We can see that the Raman noise increases with increasing fibre length until it is near the predicted maximum of 23.5 km. In the experiments that follow, we have

chosen fiber lengths that allow the strength of the Raman scattering at a given wavelength to be varied in order to isolate the effects of different impairments.

## 3. Experiment

To allow us to explore the transmission impairments discussed in the previous section, we constructed a reconfigurable link consisting of two main parts described below: the QKD system, and the optical networking system used to combine, transmit, and separate the classical and quantum signals. In order to identify the transmission impairments which affect QKD performance, additional noise measurements are made in the QKD passband (with the QKD system disconnected from the experiment), using a commercial single-photon counting system (Princeton Lightwave PGA-600).

### *3.1 QKD system*

The QKD measurements are taken with a system developed at Los Alamos for optical networking experiments [25]. It implements BB84 [4] using weak coherent pulses and phase-based encoding. The QKD wavelength is 1549.32 nm, corresponding to a channel on the ITU-standard wavelength grid. The average photon number per pulse, $\mu$, is set using a calibrated variable optical attenuator (VOA) inside Alice. The detectors are InGaAs avalanche photo diodes, cooled to 210 K. The detectors are gated at the system transmitter rate of 10 MHz and utilize after-pulse blocking. While the QKD system has been described elsewhere [25,26], it is worth noting that it uses Rb clocks at Alice and Bob to allow quantum clock recovery of the quantum signal. As a result it does not require an additional optical wavelength, bright-pulse time slot, or GPS for synchronization. Finally, although the qubits are phase encoded, the phase modulators themselves are polarization sensitive. In order to align the quantum signal polarization with that of the phase modulator at the receiver's input, a polarization controller is periodically varied to maximize the quantum signal detected after a polarizer. A complete QKD protocol stack is implemented which includes error correction [27], privacy amplification [28] and authentication [29].

### *3.2 Networking System*

As shown in figure 3, the components added to the QKD system to perform coexistence experiments consist of a bank of cw lasers, polarization controllers (PC), a ROADM network element for multiplexing and demultiplexing the optical channels, a fibre-based polarizing beam splitter (PBS), fibre spools, and additional optical passband filters preceding Bob's detectors. A ROADM network element placed at a node allows the individual wavelengths on an incoming fibre to be accessed, routed to another node, or dropped locally and possibly replaced by a new signal added at that wavelength. This is accomplished in two sections. In the first, or '*drop*' section, the wavelengths on an incoming fibre are demultiplexed and pass through a fabric of 2x2 switches which choose the 'express' (pass-through) or *drop* output independently for each wavelength. In the second, or '*add*' section, another set of 2x2 switches allows each dropped wavelength to be replaced by an added injected signal. The wavelengths are then multiplexed into an outgoing fibre. Optical taps are also used to monitor the power levels at the input, drop, add, and output ports. Our experiments represent the situation where all channels (classical and quantum) are added via separate fibres at an *add* section, multiplexed together and transmitted through a fibre, and then demultiplexed and dropped onto separate fibres at a *drop* section. The signal path thus consists of the *add* section of a ROADM, a transmission fibre, and the *drop*

section of an identical ROADM. This architecture represents a single hop between adjacent nodes on an optical ring carrying DWDM traffic.

In these experiments, we use up to three channels simultaneously of an eight-channel ROADM with 200 GHz (~1.6 nm) channel spacing. The full width at half maximum (FWHM) bandwidths are slightly narrower than the channel spacing to ensure sufficient channel-to-channel isolation. Routing within the ROADM is accomplished using MEMS-based switch fabrics. The quantum channel is fixed at 193.5 THz (1549.32 nm), the highest frequency supported by the ROADM, and various combinations of classical signals are used to investigate propagation impairments. Note that while our ROADM does not contain optical amplifiers, some ROADMs do and therefore would need to be modified to provide an amplifier bypass [30] to be used with quantum signals.

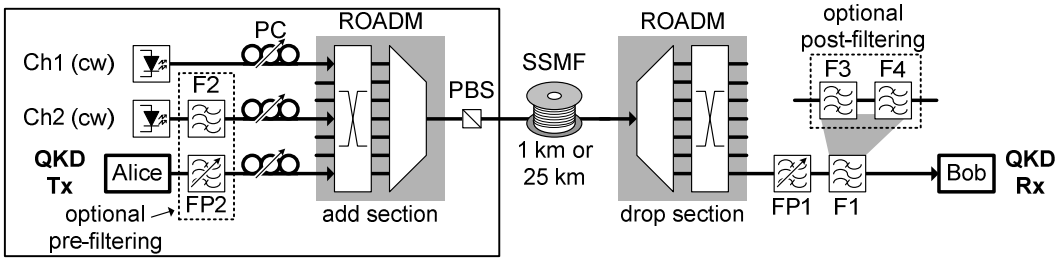


**Figure 3**. Experimental setup used for classical-quantum coexistence (see text for details). Ch1 and Ch2 are the continuous wave (cw) lasers emulating classical channels. Polarization controllers (PC) and a polarizing beam splitter (PBS) set the initial polarization. F1-F4 are fixed filters and FP1 and FP2 are Fabry-Perot tunable filters.

Alice's enclave is illustrated by the left hand side box in figure 3 and includes her QKD system, the *add* section of the ROADM and a polarizing beam splitter to ensure consistent initial launch polarizations of all signals which are aligned using polarization controllers. The classical and quantum channel powers are set at the output of the polarizing beam splitter. Although the mux and demux filters in the ROADM *add* and *drop* sections provide good isolation for classical DWDM networking (>28 dB for adjacent channels, >45 dB for non-adjacent channels), they do not provide sufficient isolation to distinguish the quantum signal from adjacent channel crosstalk. In addition, the filtering bandwidth is quite wide (~140 GHz at FWHM). It was necessary to add a multi-stage narrowband optical filter just before Bob's input to remove excess wideband noise that would otherwise be seen by the single-photon detector(s).

The experimental setup contains a ~15-GHz FWHM bandwidth Fabry-Perot filter (FP1) added to the ROADM drop, followed by a 200-GHz DWDM fixed filter (F1). The architecture also includes optional pre- and post-filtering stages depending on the requirements of the experiment. Optional pre-filtering consists of a 100-GHz pre-filter (F2) added to channel 2 and a Fabry-Perot (FP2, 5 GHz FWHM bandwidth) added to the quantum channel before they are multiplexed together. FP2 conditions Alice's laser pulse to better match the filter transfer function of the drop, before the quantum signal is launched from her enclave. The FP2 loss is internal to Alice, and can therefore be compensated by reducing the attenuation in the VOA, while maintaining the photon number at the same level. FP2 eliminates a significant portion of the spectrum from Alice's laser which would otherwise contribute to the photon number calibration but not to the number of events detected at Bob. Optional post-filtering replaces F1

with a pair of identical 100-GHz DWDM filters (F3 and F4). Optional pre- and post-filtering reduces the drop loss by ~3.2 dB, primarily attributed to the improved conditioning of Alice's laser spectrum. The total quantum signal transmission through the drop using the optional filtering and 1 km fibre is ~20% (~7 dB loss).

*3.3 Noise Measurements with Single-Photon Detectors*

To measure the characteristics of the noise generated by strong classical channels , we perform single-photon measurements of the noise falling within the quantum channel passband at Bob's input while the QKD signal is absent. As we have previously demonstrated [31], by using the high-isolation optical filtering techniques employed here, one can suppress the linear crosstalk resulting from adjacent and non-adjacent DWDM channels to negligible levels. Once the cross talk is mitigated, the dominant noise terms remaining are spontaneous Raman scattering and four-wave mixing (FWM) noise [31, 32], which as discussed in previous sections are generated as a result of the propagation of one or more strong classical channels over a fibre link. Although both sources of noise can be present simultaneously, we have selected system parameters (fibre type and length, DWDM channel power, and DWDM channel spacing) to operate in regimes where either FWM or spontaneous Raman scattering is the *dominant* noise term, in order to highlight their differences in dependency on total classical power. We measure the resulting noise with an InGaAs APD-based single-photon detector. The detector is gated at a 500 kHz rate, with 1-ns gates, and an after-pulse blocking period of 12 μs following each avalanche. The detector dark count rates are ~240 per measurement interval and are subtracted from the output. Measurements are taken using two different transmission lengths of standard single mode fibre (SSMF) of 1 km and 25 km. All laser polarizations are aligned with respect to the transmission port of the PBS, ensuring repeatable worst-case contributions from any FWM products. Various combinations of signals are launched into the ROADM *add* ports in order to compare single-channel and multi-channel effects as classical channel launch power levels are varied.

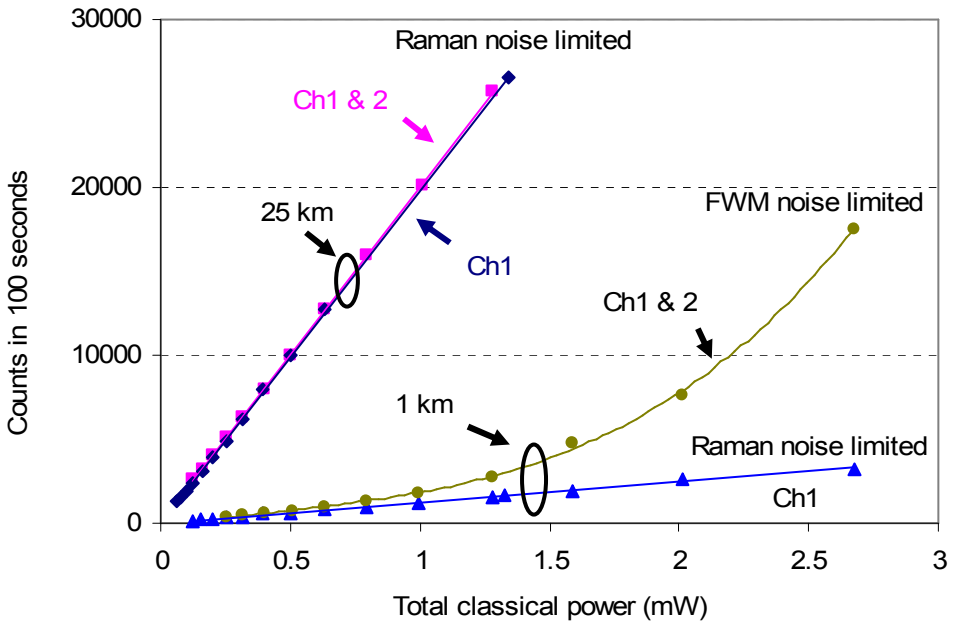


**Figure 4.** Noise at Bob's input using the optional pre- and post-filtering measured with a commercial InGaAs single photon counting system. Alice's quantum signal was disconnected

during these measurements. The noise linearly increases with increasing total channel power for most plotted configurations which is consistent with what one would expect from Raman noise as predicted in equation (9). The one exception is when Channels 1 & 2 are simultaneously launched into the 1 km fibre, where the response and fit are cubic, in agreement with FWM equation (2). Error bars from Poisson counting fluctuations are smaller than the size of the data points. (Note the x-axis represents the sum of the power of the individual channels when Ch1 and Ch2 are present.)

The results of the photon counting measurements are summarized in figure 4, which shows several series of dark-count subtracted 100-second noise measurements. Channel 1 (Ch1) and channel 2 (Ch2) have frequencies of 193.1 THz (1552.52 nm) and 193.3 THz (1550.92 nm), respectively. When only a single channel is present in either the 1-km or 25-km fiber, the photon count rate increases linearly with the launched classical channel power, as is expected from spontaneous Raman scattering [31]. In contrast, when both channels are transmitted through the 1-km fibre, the noise increases nonlinearly and much more rapidly with the total power. Thus with the addition of Ch2, the FWM noise term is now present [32] and actually becomes the dominant noise source over Raman scattering as evidenced by the approximately cubic dependence on DWDM channel power seen in figure 4. However, when both Ch1 & Ch2 are present in the 25 km fibre, for this particular selection of channel spacing and SSMF fibre dispersion, the spontaneous Raman scattering dominates over the FWM since we are near the peak Raman noise accumulation length (previously shown to be ~24 km). As a result, the noise measurements when both DWDM channels are launched into a 25-km SSMF link are approximately linear with increasing total classical channel power.

## 4. Impact of noise on QKD system performance

In this section, we discuss the impact of FWM and spontaneous Raman noise generated by multiplexed classical channels on QKD performance parameters, which include the quantum bit error rate (QBER) and secret key rate. After adding the QKD system described in 3.1 to the networking system of 3.2, we investigated several classical channel configurations and fibre lengths designed to isolate the various parameters responsible for the dominant noise effects. These experiments utilize a mean photon number of $\mu$=0.4 photons per pulse. We record the QBER and secret key rate, using a typical average of 25 QKD runs for each point in the plotted data. The results of the QKD experiments with the ROADM are shown in figures 5 through 8, where the data consists of QKD runs below a maximum QBER threshold of 11%. In part (a) of the figures, the QBER is plotted as a function of the total power launched into the fibre, while part (b) plots the corresponding secret key generation rates. The classical power is increased until the key generation performance drops sharply. Here we explore the impairments generated using per channel launch powers of ~0.08 mW to ~ 3 mW (-11 dBm to +4.8 dBm). The error bars are the calculated standard deviation of the data.

### *4.1 Four-wave mixing in 1 km of fibre*

In consideration of equation (9) and figure 1, a 1-km SSMF fibre is short enough to minimize the Raman noise generated but still long enough to study the effects of FWM. The first experiment demonstrates the impact of increasing the power of Channels 1 and 2 on QKD system performance, with a 1 km fibre. We use it as a baseline experiment, the results of which are replotted for comparison in several of the other plots from this subsection. We also plot the results when only Channel 2 is on, to provide a comparison of the two-channel performance with the single-channel case. All of the polarizations (for both quantum and classical channels, unless otherwise noted) are aligned with the PBS so that the worst-case FWM noise is generated.

In figure 5 (a) and (b), we plot the QKD system performance as a function of increasing power, which is split equally between Channels 1 and 2. This 200 GHz spaced experiment sets channel 1 (Ch1) and channel 2 (Ch2) at frequencies of 193.1 THz (1552.52 nm) and 193.3 THz (1550.92 nm), respectively. The results in figure 5 (a) show a strong nonlinearity in the QBER as the total power is increased. In contrast, nonlinear behaviour in the QBER is not observed when only Channel 2 is present (with the same total power as the Channels 1 and 2 combined). The secret key rate falls off sharply as a function of increasing power when Channels 1 and 2 are simultaneously on, due to the sharp rise in the QBER. By comparison, only a relatively minor degradation in secret bit rate is observed when only Channel 2 is present. This minor impairment from a single classical channel indicates that there is sufficient isolation of channel 2 from the quantum channel to allow observation of the nonlinear effects of FWM. When operating Channels 1 and 2 at a total power of 1.58 mW, the QKD system is just able to perform QKD with a key rate of 73 ± 96 bits per second. However, by the time the classical power reaches 2 mW, the QKD system is not able to generate any secret key bits due to the FWM impairment, thus the performance is dropping off very quickly for combined classical channel power of 1.58 mW.

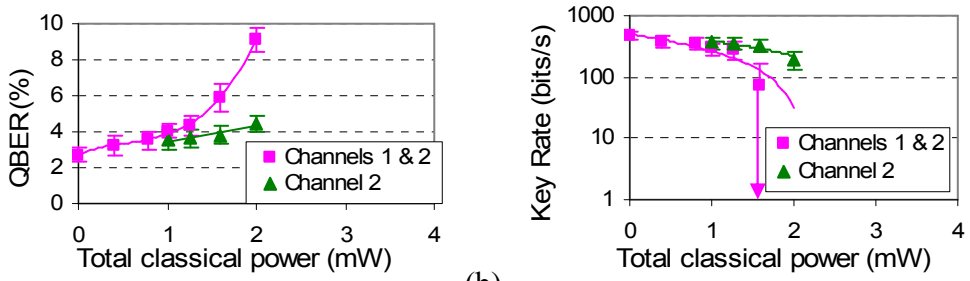


**Figure 5.** QKD performance is plotted as a function of total cw laser power launched into the same 1-km fibre as the quantum signal (see text). Lines are drawn to help guide the eye. Note that the key rate for the 200 GHz spaced channels (shown as squares in the plots above) at 1.58 mW has a lower error bar overlapping zero which is not plotted above but is indicated with an arrow. Additionally, the zero secret bit result for the 200 GHz spacing produced at 2 mW is not plotted on this log scale.

In the second experiment of this subsection, the channel plan remains unchanged but, the classical signals are launched with their polarizations aligned with each other, but orthogonal to that of the quantum channel. The two classical channels are muxed together and added into the orthogonal polarization PBS input port with respect to the quantum signal polarization. This tests one possible method of suppressing the strong FWM product, which is co-polarized with the classical channel pumps, by later rejecting it through polarization filtering at the QKD receiver. The results of increasing the power of Channels 1 and 2 simultaneously when co-polarized (replotted from figures 5 (a) and (b)) and cross-polarized relative to the QKD channel are shown in figure 6 (a) and (b). The data show that this type of polarization multiplexing helps suppress the co-polarized FWM product by taking advantage of the QKD system design. Bob's receiver passes only a single polarization and therefore suppresses a significant fraction of the FWM component aligned to the classical signals since it is (predominantly) orthogonal to the QKD channel. Thus using classical signals which are cross-polarized with the classical channel suppresses the effect of FWM resulting in a linearly increasing error rate with increasing classical channel power.

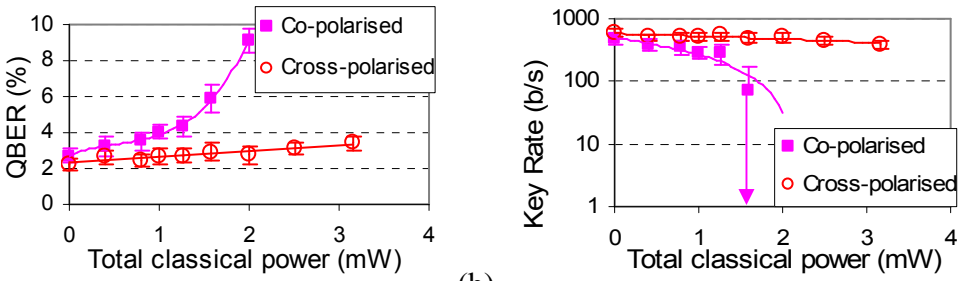


(a) (b)

**Figure 6.** QKD performance is plotted as a function of two cw laser channels with equal powers launched into the same 1-km fibre as the quantum signal. This plot shows that launching the classical signals in an orthogonal polarization mode to that of the quantum signal can be used to suppress the effects of FWM.

In the final FWM experiment, we fix all polarizations so that they are identical upon launch and examine the impact that the classical channel plan has on the performance of the quantum channel. In figures 7 (a) and (b), we plot the baseline results for two equal strength classical channels on the 200 GHz grid, along with the corresponding results for a 400 GHz grid (obtained by skipping every other channel in the ROADM). Thus the two classical channels are centred at frequencies of 192.7 THz (1555.75 nm) and 193.1 THz (1552.52 nm), creating a 400 GHz grid with the quantum channel at 193.5 THz. Figure 7 (a) shows the nonlinear increase in the QBER when using the 200 GHz spacing, but only a linear increase in QBER in the 400-GHz spaced cases. As we mentioned earlier, moving from a 200 GHz channel spacing to 400 GHz in a 1-km SSMF link theoretically results in a decrease of FWM noise by approximately 10 dB. In this example, FWM is no longer the dominant noise term, even for a 1 km fibre length.

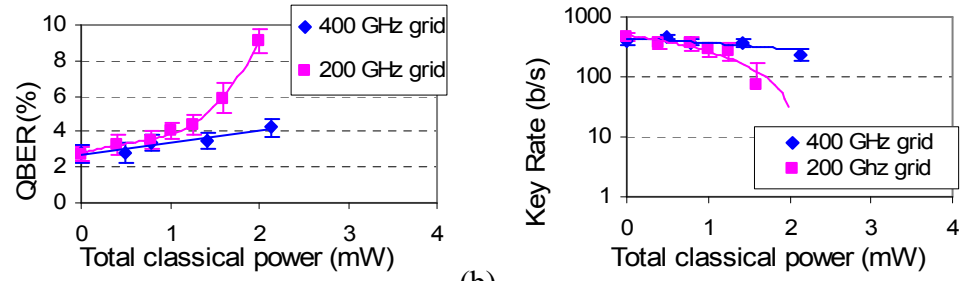


(a) (b)

**Figure 7.** QKD performance is plotted as a function of two cw laser channels with equal powers launched into the same 1-km fibre as the quantum signal. This plot demonstrates that larger channel spacing can mitigate the effect of FWM impairments.

We have demonstrated several strategies that can be useful for mitigating the impact of FWM impairments on QKD performance, even when operating with relatively high classical channel power levels. These include polarization multiplexing and operation with wider channel spacing. Other experiments were performed such as skipping a channel between the QKD and classical channels (which in this case keeps QKD outside of the frequency range of the FWM products). These results also gave a similar performance to the 400 GHz grid data. Overall, these experiments show the impact of FWM on QKD signals multiplexed closely with classical signals. The FWM impairment occurs when the classical channel powers are relatively high, in this case >

1 mW of total power. However, in many practical cases involving short distances, the classical launch power will be much less and FWM will not necessarily be an impairment.

*4.2 Coexistence over 25 km of fibre*

In this subsection, we move to a 25 km fibre length, a more useful distance than 1 km for metro and enterprise networks. Considering that 25 km is very close to where Raman noise is a maximum for this fibre type and the FWM noise is suppressed by an order of magnitude from the 1-km case (as predicted in figure 1), this is an excellent configuration to explore the effect of Raman noise in relative isolation of FWM. The 25-km fibre measurements in figure 8 (a) and (b) utilize the optional pre- and post-filters shown in figure 3. Other than the filtering improvements and the increased fibre length, the experiment is carried out in the same manner as the FWM experiments using 200 GHz channel spacing. The total classical power is varied when both Channels 1 and 2 are launched into the fibre, and also when each channel is separately turned on. It should be noted that the Raman noise reaches a peak at a frequency difference of approximately ± 1700 GHz from the carrier. The 200 GHz channel spacing here does not represent the worst case scenario. Additional channels added to the ROADM that are greater than or equal to ~1700 GHz from the QKD system or larger channel spacing than the one considered here will create even more noise increasing the impairment to the QKD system.

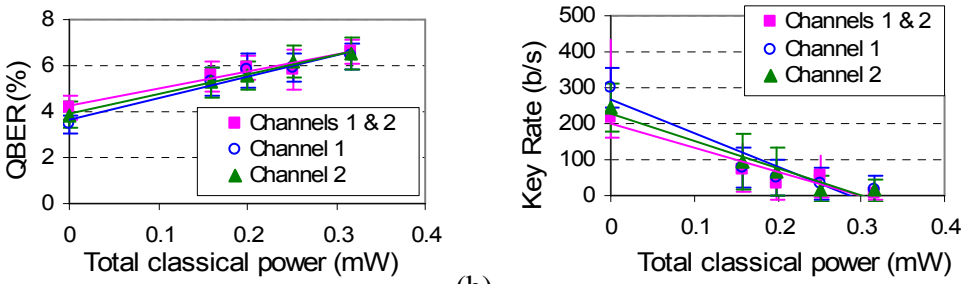


(a) (b)

**Figure 8.** QKD performance is plotted as a function of total cw laser power launched into the same 25-km fibre as the quantum signal (see text). In (b), the secret bit rate is fitted to a line to guide the eye. Due to the relatively small spread in QKD secret bit rates, it is unnecessary to plot the data on a vertical log scale as in figure 3. The differences in the data at zero power are due to small systematic errors.

In contrast to the 1-km case, the data shows a linear increase in QBER with increasing channel power, independent of which classical channel or channels are on. When both channels equally share the launched power, the impairment is the same as when either individual channel is turned on with the same total power. In this case, the QKD system performance is limited by the spontaneous Raman noise. Note that this Raman noise limit does not preclude the presence of FWM noise at a lower level. However the 25-km Raman noise is much stronger than either the Raman noise or the FWM noise for the 1-km fibre case, as is evident from single-photon counting data previously described in figure 4. This behavior is expected for standard single mode fibre because 25 km is very close to the distance at which the Raman noise is a theoretical maximum as discussed above. In addition, from figure 1, the expected theoretical FWM noise after 25 km is an order of magnitude lower than for the 1 km case. When one considers that the FWM strength decreases and the Raman noise increases when switching from 1 km to 25 km, the different curves in figure 4 qualitatively agree with expectations. In the presence of two 0.16 mW (-8 dBm) classical channels through 25 km of fibre and a ROADM on a 200 GHz grid, the QKD

system occasionally produces final key bits at an average rate of 6 bits per second over approximately 25 runs.

*4.3 Considerations for other fibre types and data modulation*

In the previous sections, we explored the impact of Raman and FWM transmission impairments over both 1 km and 25 km SSMF links. Although the range of the applications where 1 km links can be found is limited, it enables us to clearly illustrate regimes where FWM fibre impairments can dominate, while spontaneous Raman scattering is not a significant impairment. In addition, if one considers other common fibre types (such as non-zero dispersion-shifted fibre), FWM can have a larger impact over distances longer than 1km. For example, the FWM noise for a 25-km NZ-DSF link is approximately 20 dB higher than for a 25-km SSMF link, as seen in the calculations plotted in figure 1. As a result, FWM can quickly become the dominant impairment in low dispersion fibres. This will be the subject of further study.

For simplicity, we utilized unmodulated cw lasers to emulate DWDM network channels. Previous studies have investigated the difference between cw and the most common modulation format in optical networks, non-return-to-zero on-off-keying (NRZ-OOK). It was shown that NRZ-OOK modulated signals generate comparable FWM power to cw signals due to a balancing between the higher peak power and the pulse walk-off between the modulated waveforms [33]. Therefore, our results should be representative of links with NRZ-modulated data. However, the use of modulation formats other than NRZ can help to reduce FWM. As an example, in [34], duobinary modulation was employed to reduce the strength of FWM by 1 to 3 dB, in transmission over a 20 km dispersion-shifted fibre (DSF).

## 5. Conclusions

Commercial optical networks are increasingly adopting multi-channel DWDM technology in the 1.5-μm band. This trend is driven by the lower fibre attenuation, the availability of optical fibre amplifiers, and inexpensive DWDM components at standard wavelengths. While in this work the focus has been on understanding the limits and requirements when adding quantum channels in the 1.5-μm window, we have also previously demonstrated network coexistence with QKD signals in the 1.3-μm band [12, 20]. In many cases, operating QKD in the 1.3-μm window may be a more attractive solution for shared quantum/classical networks, due to the larger wavelength separation between the strong and weak signals. This configuration allows compatibility with amplified transmission links (with QKD bypassing the optical amplifiers), reduces backgrounds from Raman scattering, and eliminates FWM as a major concern. However, there are also situations in which 1.5-μm QKD may be more favourable, depending on the application, the type of network, and the choice of system parameters (DWDM channel power, channel count, fibre dispersion, etc.). Therefore to understand under what conditions one may successfully send quantum communications signals along the same fibre with high-power closely spaced 1.5-μm classical signals, we have mapped out the noise mechanisms in this regime.

In addition we have shown the impact of FWM and Raman noise on quantum communications and, more specifically BB84 QKD. We demonstrated 1.5-μm classical-quantum coexistence through ROADMs, an optical networking technology that increases the flexibility, transparency and reconfigurable connectivity of quantum and classical networks. We calculated the impact of four-wave mixing for a variety of channel spacings, fibre types, and distances. We measured QKD performance in two regimes where the noise limiting factor is dominated by different mechanisms, including FWM over a 1-km fibre and Raman scattering over a 25-km standard single-mode fibre. We demonstrated and discussed several strategies that can be used to mitigate FWM impairments on the quantum channel, including polarization multiplexing and increased channel spacing. However, in situations where Raman noise is the dominate

impairment, it is not easily decreased on existing networks where classical channel launch powers are fixed. Therefore managing Raman-noise impairments remains a key challenge to the integration of quantum communications into the existing optical communications infrastructure. By exploring the quantum channel impairments generated from classical channels, and how those impairments may be mitigated through network planning, these results lay the groundwork for defining requirements for successfully enabling quantum-classical coexistence in C-band reconfigurable optical networks. The present work represents an important step towards developing a broader understanding of these tradeoffs, and of the most attractive domains of use for QKD and other types of quantum communications in shared quantum/classical networks.

**Acknowledgements**
This work was supported by IARPA and hosted by the LTS.

**References**

[1] Berthold J, Saleh A A M, Blair L and Simmons J M 2008 *J. Lightwave Tech.* **26** 1104

[2] Xia T J *et al* 2008 *Optical Fiber Communication Conference* NMC2

[3] Wiesner S. 1983 *SIGACT News* **15** 78

[4] Bennett C H and Brassard G 1984 *Proc. IEEE Int. Conf. on Computers, Systems, and Signal Processing (Bangalore)* (New York: IEEE) 175

[5] Franson J D and Ilves H 1994 *App. Opt.* **33**, 2949

[6] Muller A, Zbinden H and Gisin N 1996 *Europhys. Lett.* **33** 335

[7] Townsend P D 1997 *Electron. Lett.* **33** 188

[8] Hughes R G, Morgan G and Peterson C 2000 *J. Mod. Opt.* **47** 533

[9] Elliott C, Pearson D and Troxel G 2003 *SIGCOMM '03: Proc. of the 2003 Conf. on Applications, technologies, architectures, and protocols for computer communications (Munich)* (New York: ACM) 227

[10] Toliver P *et al* 2003 *IEEE Photon. Technol. Lett.* **15** 1669

[11] Poppe A *et al* 2004 *Opt. Exp.* **12** 3865

[12]Yuan Z and Shields A 2005 *Opt. Exp.* **13** 660

[13] Runser R J, *et al* 2005 *Optical Fiber Communication Conference* OWI2

[14] Namekata N, Mori S and Inoue S 2005 *Opt. Exp.* **13** 9961

[15] Xia T J, Chen D Z, Wellbrock G, Zavriyev A, Beal A C and Lee KM 2006 *Optical Fiber Communication Conference* OTuJ7

[16] Tajima A, Tanaka A, Maeda W, Takahashi S and Tomita A 2007 *IEEE J. Selected Topics in Quant. Elect.* **13** 1031

[17] Ma L, Chang T, Mink A, Slattery O, Hershman B and Tang X 2007 *IEEE Com. Lett.* **11** 1019

[18] Chen W *et* al 2007 *Preprint* quant-ph/0708.3546

[19] Poppe A, Peev M and Maurhart O 2008 *Int. J. Quant. Inf.* **6** 209

[20] Chen T-Y *et al* 2008 *Preprint* quant-ph/0810.1264

[21] Chapuran T E *et al* 2008 to be submitted to *New J. Phys.*

[22] Agrawal G P *Fiber-Optic Communication Systems* (New York: Wiley)

[23] Forghiere F, Tkach R W and Chraplyvy 1997 *Chapter 8 in Optical Fiber Telecommunications* IIIA vol A, ed I P Kaminow and T L Koch (San Diego: Academic) 196

[24] Mandelbaum I and Bolshtyansky M 2003 *IEEE Photonics Tech. Lett.* **15** 1704

[25] Hughes R J *et al* 2005 *Proc. SPIE* **5893** 589301

[26] Hiskett PA, Rosenberg D, Peterson C G, Hughes R J, Nam S, Lita A E, Miller A J and Nordholt JE 2006 *New J. Phys.* **8** 193

[27] Brassard G and Salvail L 1994 *Lecture Notes Comput. Sci.* **765** 410

[28] Gottesman D, Lo H-K, Lutkenhaus N and Preskill J 2004 *Quantum Inf. Comput.* **4** 325

[29] Wegman M N and Carter J L 1981 *J. Comp. Sys. Sci.* **22** 265

[30] Nweke N I *et al* 2006 *Conference on Lasers and Electro-Optics (CLEO '06)* CWQ7

[31] P Toliver *et al* 2004 *IEEE Lasers and Electro-Optics Society 2004 (LEOS '04)* **2** 491

[32] Toliver P *et al* 2007 *Conference on Lasers and Electro-Optics (CLEO '07)* CaThBB1

[33] Song S, Allen C, Demarest K, Pelz L, Fang X and Pua Y 1997 *IEEE Lasers and Electro-Optics Society 1997 (LEOS '97)* **2** 224

[34] Katsaros G, Lane P, Murphy M, Green M and Jiang P 2000 *London Communications Symposium;* http://www.ee.ucl.ac.uk/lcs/papers2000/lcs078.pdf